Mon. Not. R. Astron. Soc. **397,** 569–576 (2009) doi:10.1111/j.1365-2966.2009.14997.x

Revisiting the relativistic ejection event in XTE J1550−564 during the 1998 outburst

D. C. Hannikainen,[1⋆] R. W. Hunstead,[2] K. Wu,[3] V. McIntyre,[4] J. E. J. Lovell,[5] D. Campbell-Wilson,[2] M. L. McCollough,[6] J. Reynolds[4] and A. K. Tzioumis[4]

[1]*Metsähovi Radio Observatory, TKK, Metsähovintie 114, FI-02540 Kylmälä, Finland*
[2]*Sydney Institute for Astronomy, School of Physics, University of Sydney, NSW 2006, Australia*
[3]*Mullard Space Science Laboratory, University College London, Holmbury St Mary, Dorking, Surrey RH5 6NT, UK*
[4]*ATNF, CSIRO, PO Box 76, Epping, NSW 1710, Australia*
[5]*School of Mathematics & Physics, Private Bag 21, University of Tasmania, Hobart TAS 7001, Australia*
[6]*Harvard–Smithsonian Center for Astrophysics, 60 Garden Street, Cambridge, MA 02138, USA*

Accepted 2009 April 28. Received 2009 April 21; in original form 2009 February 6

ABSTRACT

We revisit the discovery outburst of the X-ray transient XTE J1550−564 during which relativistic jets were observed in 1998 September, and review the radio images obtained with the Australian Long Baseline Array, and light curves obtained with the Molonglo Observatory Synthesis Telescope and the Australia Telescope Compact Array. Based on HI spectra, we constrain the source distance to between 3.3 and 4.9 kpc. The radio images, taken some 2 d apart, show the evolution of an ejection event. The apparent separation velocity of the two outermost ejecta is at least $1.3c$ and may be as large as $1.9c$; when relativistic effects are taken into account, the inferred true velocity is $\geq 0.8c$. The flux densities appear to peak simultaneously during the outburst, with a rather flat (although still optically thin) spectral index of −0.2.

Key words: stars: individual: XTE J1550−564 – radio continuum: stars – radio lines: stars – X-rays: binaries.

1 INTRODUCTION

The soft X-ray transient XTE J1550−564 was discovered by the All-Sky Monitor (ASM) on board the *Rossi X-ray Timing Explorer* (*RXTE*) on MJD 51063 (1998 September 7; MJD = JD−240000.5) with an intensity of ∼0.07 Crab in the 2–12 keV range (Smith 1998) and by the Burst and Transient Source Experiment (BATSE) on the *Compton Gamma-Ray Observatory* (*CGRO*). The flux in the 20–100 keV range showed an impulsive rise, increasing from $< 0.1 \times 10^{-8}$ to 2.42×10^{-8} erg s^{-1} cm $^{-2}$ between MJD 51063 and 51066 (Wilson et al. 1998). The *RXTE*/ASM intensity increased steadily over the next few days, reaching ∼1.7 Crab on MJD 51071 (Remillard et al. 1998). XTE J1550−564 flared to 6.8 Crab on MJD 51075–51076, making it the brightest X-ray nova observed with *RXTE* to date (Remillard et al. 1998).

On MJD 51065, an optical counterpart with a magnitude of $V = 16$ was identified (Orosz, Bailyn & Jain 1998), and a radio counterpart was discovered at the optical position with a flux density of 10 ± 2.5 mJy (Campbell-Wilson et al. 1998). An orbital period of ∼1.54 d was attributed to the system (Jain et al. 2001). Orosz et al. (2002) have found dynamical evidence for a black hole in XTE J1550−564. Based on optical spectra of the companion star (the dereddened colour suggests spectral type G/K), they find that the most likely value of the mass of the compact object lies in the range $8.63 \leq M_1 \leq 11.58\,\mathrm{M}_\odot$, which is well above the maximum mass of a stable neutron star.

XTE J1550−564 showed a relativistic ejection event in the radio wavebands during the 1998 outburst (Hannikainen et al. 2001). A gradual deceleration in the relativistic jets was inferred from Australia Telescope Compact Array (ATCA) observations in 2000 and 2002 (Corbel et al. 2002). The radio data are consistent with a synchrotron origin for the emission from the jets. The jet components of XTE J1550−564 were seen also in *Chandra* images (Corbel et al. 2002; Kaaret et al. 2003; Tomsick et al. 2003). Interestingly, the extrapolation of the radio spectrum to the X-ray wavelengths is consistent with the X-ray flux density derived from the *Chandra* observations at similar epochs. If the X-ray emission is direct synchrotron emission from the same population of relativistic electrons that gives rise to the radio emission, the energies of these electrons must reach ∼10 TeV (Corbel et al. 2002). This scenario requires a very efficient acceleration mechanism operating in XTE J1550−564 so as to populate the electrons in the very high-energy ranges.

Timing analysis showed evolving X-ray quasi-periodic oscillations (QPOs) (Cui et al. 1999; Titarchuk & Shrader 2002) and hard

⋆E-mail: diana@kurp.hut.fi

lags (Wijnands, Homan & van der Klis 1999), similar to those often seen in other black hole binaries. The source also showed non-trivial X-ray spectral variability, spectral state transitions and probably hysteresis during the 1998 and 2000 outbursts (Corbel et al. 2001; Homan et al. 2001; Kubota & Done 2004; Wu, Liu & Li 2007; Xue, Wu & Cui 2008). In the 2–30 keV range, the spectra could generally be fitted by a three-component model, consisting of a thermal (multicolour) disc, a power law and a 6.4 keV Gaussian line component (Sobczak et al. 1999; Kubota & Done 2004), but the relative strengths of the components changed as the outburst proceeded. The origin of the X-rays from XTE J1550−564 is the subject of much debate. Some suggest that the X-rays (at least the large-scale jet components) are direct or Comptonized synchrotron emission (see e.g. Tomsick et al. 2003; Wang, Dai & Lu 2003; Corbel, Tomsick & Kaaret 2006). On the other hand, for the X-ray bright case at least, a recent study based on *Chandra* and *RXTE* data argues that the keV X-rays are mainly emissions arising from the accretion flows (Xue et al. 2008).

The 1998 outburst of XTE J1550−564 can be divided into five phases based on the morphology of the X-ray light curve observed by *RXTE*/ASM. The phases are characterized by (i) a fast rise in the X-ray flux, (ii) a slower rise in the X-ray flux, (iii) a giant flare, (iv) a period of standstill in the flux and (iv) an exponential-like decay (Wu et al. 2002). At the onset of the outburst, the initial rise in the hard (20–100 keV) X-ray flux was impulsive, which can be seen in the BATSE data. The rise in the soft (<20 keV) X-ray flux was, in contrast, less rapid. The difference in the rise times of the soft and hard X-rays can be attributed to the accreting matter having two different distributions of angular momenta (see Beloborodov & Illarionov 2001; Smith, Heindl & Swank 2002; Wu et al. 2002). While matter with low angular momentum surges into the black hole on a free-fall time-scale, matter with higher angular momentum diffuses inward forming a viscous accretion disc. A possible scenario for the mass transfer in XTE J1550−564 was proposed by Wu et al. (2002), which explains the co-existence of material with high- and low-angular momenta that gives rise to the respective soft and hard X-ray bursts.

Here, we present radio observations of XTE J1550−564 during the 1998 September outburst. The paper is organized as follows. In Section 2, we show the technical details and the results of the radio observations; in Section 3, we compare the radio outburst behaviour of XTE J1550−564 with that of another Galactic superluminal source, GRO J1655−40. A summary is given in Section 4.

2 RADIO OBSERVATIONS

The initial radio detection of XTE J1550−564 was made on MJD 51065 with the Molonglo Observatory Synthesis Telescope (MOST) of the University of Sydney. The MOST observed the source on 12 occasions at 843 MHz between MJD 51065 and 51092, while the ATCA observed it at 1.4, 2.3, 4.8 and 8.6 GHz between MJD 51073 and 51085. Very long baseline interferometry (VLBI) images were obtained with the Australian Long Baseline Array (LBA) at 2.29 and 8.4 GHz about 15 d after the first detection (MJD 51080–51082).

2.1 MOST and ATCA

The MOST operates on the principle of earth-rotation aperture synthesis at a frequency of 843 MHz. It is a 1.6 km east–west array, consisting of two cylindrical paraboloids of dimension 778 × 12 m^2 separated by a gap of 15 m, giving a resolution of 43 × 43 cosec $|\delta|$ arcsec^2 (Mills 1981; Robertson 1991).

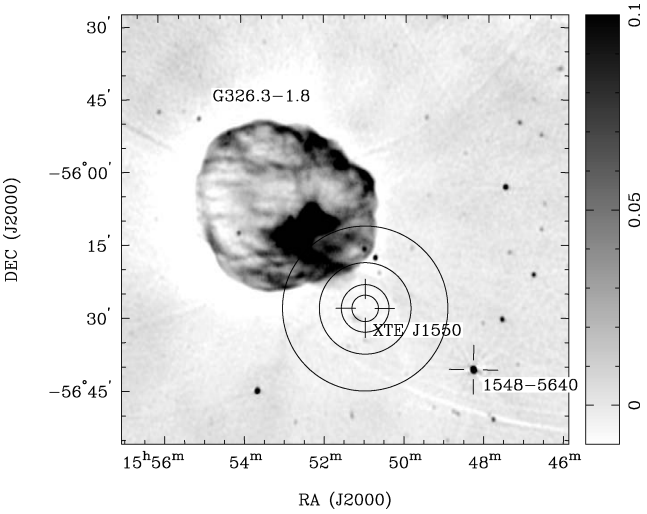

Figure 1. The MOST image at 843 MHz, showing the ATCA fields of view at 1.4, 2.3, 4.8 and 8.6 GHz at the position of XTE J1550−564 and the supernova remnant G326.3−1.8. To the lower right is SUMSS J154816−564057, used as the reference source for estimating the distance to XTE J1550−564 (see Section 2.2).

Following the initial detection of XTE J1550−564, the source was monitored over the following 27 d resulting in 12 observations, using partial synthesis observations with integration times ranging from 1 to 9 h. The calibration sources used were PKS B1421−490 and B1934−638. Flux density measurements were complicated by sidelobes from the nearby radio-bright supernova remnant G326.3−1.8 (Whiteoak & Green 1996), clearly seen in Fig. 1 which shows the image of the field of XTE J1550−564 at 843 MHz. This necessitated an image differencing approach using a matched reference image of the field obtained earlier in 1998 when XTE J1550−564 was quiescent. The flux density estimates are given in Table 1, with the errors being the quadrature combination of a 3 mJy rms noise contribution and a 3 per cent calibration uncertainty.

The ATCA is an earth-rotation aperture synthesis array consisting of six 22-m antennae on a 6-km baseline, operating at that time at frequencies of 1.2–10.2 GHz with bandwidths of 128 MHz in two linear polarizations. The amplitude and bandpass calibrator was PKS B1934−638, while the phase calibrators were B1549−790 at 1.4 and 2.3 GHz, and B1554−64 at 4.8 and 8.6 GHz.

The top panel of Fig. 2 shows the MOST 843 MHz and ATCA light curves at four observing frequencies. The MOST 843-MHz light curve is reproduced here from Wu et al. (2002). Also plotted are the global two-point spectral indices calculated from the ATCA data (Fig. 2, bottom). All the radio data, including observing dates, flux densities at all five observing frequencies and global two-point spectral indices, are summarized in Tables 1 and 2.

Following the initial detection of XTE J1550−564 on MJD 51065, the MOST monitored the source at 843 MHz over the next 27 d (Fig. 2). Between MJD 51065 and 51073, the source flux density remained between 10 and 30 mJy. After MJD 51073, the flux density began to increase, reaching 168 mJy on MJD 51076, and peaking on MJD 51078 with a flux density of 375 mJy. The flux density then declined to 120 mJy over the next 3 d, with a

Table 1. Flux densities of XTE J1550−564 at all five observing frequencies. The MJD refers to mid-observation.

MOST		ATCA					
MJD	$S_{0.843}$ (mJy)	MJD	$S_{1.4}$ (mJy)	$S_{2.3}$ (mJy)	MJD	$S_{4.8}$ (mJy)	$S_{8.6}$ (mJy)
51065.18	12 ± 3						
51066.16	16 ± 3						
51071.20	27 ± 3						
51073.19	18 ± 3	51073.08	13.2 ± 1.3	13.3 ± 0.4	51073.05	10.1 ± 0.2	7.8 ± 0.2
		51073.14	11.2 ± 1.3	13.2 ± 0.4	51073.11	9.4 ± 0.2	7.6 ± 0.2
		51073.20	15.3 ± 1.2	12.1 ± 0.4	51073.17	10.6 ± 0.2	9.8 ± 0.2
		51073.26	15.5 ± 1.0	13.4 ± 0.4	51073.23	13.2 ± 0.2	12.6 ± 0.1
		51073.31	12.3 ± 1.2	16.6 ± 0.3	51073.29	14.9 ± 0.2	14.0 ± 0.1
					51073.33	14.3 ± 0.5	12.9 ± 0.5
51076.39	168 ± 6						
51077.30	327 ± 10	51077.25	320.2 ± 3.4	288.8 ± 3.1	51077.26	267.3 ± 0.7	220.4 ± 0.7
		51077.55	330.8 ± 4.7	289.4 ± 3.1	51077.55	282.9 ± 1.2	234.4 ± 1.0
					51077.56	281.3 ± 1.2	231.7 ± 1.0
51078.26	375 ± 12	51078.07	299.4 ± 3.2	292.1 ± 4.0			
		51078.10	283.5 ± 3.2	260.1 ± 2.8			
51079.32	221 ± 7	51079.41	193.2 ± 2.7	162.6 ± 0.7			
					51079.39	139.6 ± 0.2	115.0 ± 0.2
51080.30	155 ± 6	51080.25	139.0 ± 1.9	118.6 ± 0.6	51080.23	98.2 ± 0.3	76.3 ± 0.5
51081.21	120 ± 5	51081.04	99.0 ± 1.0	85.3 ± 0.5	51081.05	92.5 ± 0.3	87.9 ± 0.3
		51082.47	51.3 ± 1.3	56.0 ± 0.5	51082.50	59.9 ± 0.4	53.1 ± 0.4
		51084.09	52.8 ± 1.0	45.5 ± 0.5	51084.08	44.9 ± 0.3	
		51085.07	30.5 ± 0.9	37.8 ± 0.4	51085.06	25.0 ± 0.3	
		51086.36	23.4 ± 0.8	23.3 ± 0.3	51086.37	20.4 ± 0.1	
		51086.39	27.7 ± 0.9	23.7 ± 0.4			
51087.36	20 ± 3						
51092.18	14 ± 3						
		51109.23	6.3 ± 0.7	3.2 ± 0.3			

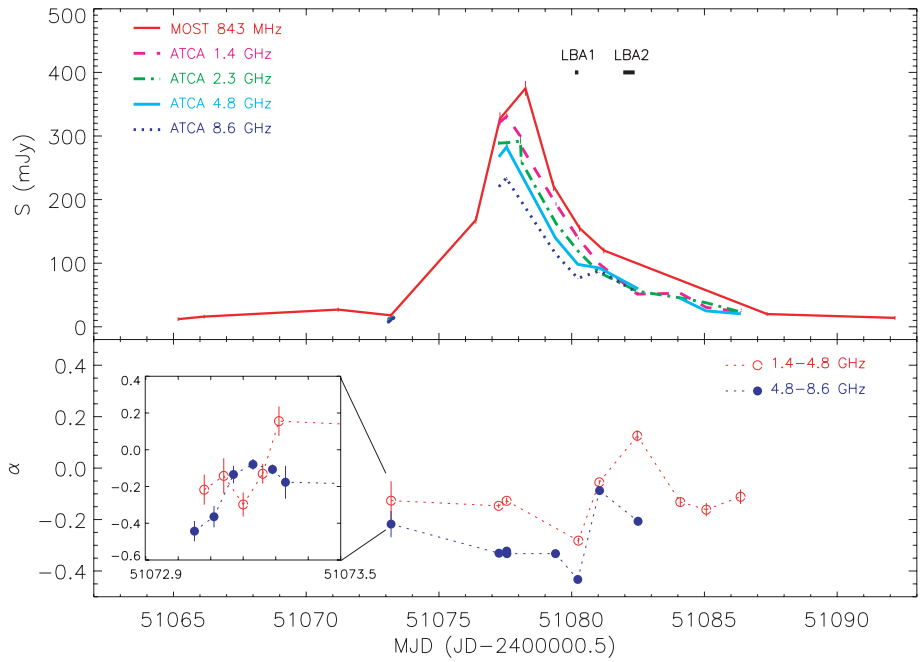

Figure 2. The MOST and ATCA light curves from 1998 September (top). The epochs (LBA1 corresponds to Epoch 1 and LBA2 to Epoch 2) and durations of the LBA observations are marked. The two-point spectral indices derived from the ATCA data are in the bottom panel. The data points at ∼MJD 51073 are an average of the first five 1.4–4.8 GHz and the first six 4.8–8.6 GHz data points, shown in the inset. The dates for the 1.4 GHz data were used in plotting the 1.4–4.8 GHz spectral indices.

Table 2. Spectral indices. The MJD refers to mid-observation.

MJD	$\alpha_{0.843-8.6}$	MJD	$\alpha_{1.4-4.8}$	MJD	$\alpha_{4.8-8.6}$
		51073.08	−0.22±0.08	51073.05	−0.44±0.06
		51073.14	−0.14±0.10	51073.11	−0.36±0.06
51073.19	−0.22±0.06	51073.20	−0.30±0.07	51073.17	−0.13±0.05
		51073.26	−0.13±0.05	51073.23	−0.08±0.03
		51073.31	0.16 ± 0.08	51073.29	−0.11±0.03
				51073.33	−0.18±0.09
		51077.25	−0.15±0.01	51077.26	−0.33±0.01
51077.30	−0.17±0.02	51077.55	−0.13±0.01	51077.55	−0.32±0.01
				51077.56	−0.33±0.01
51078.26	−0.30±0.01				
51079.32	−0.26±0.01	51079.41	−0.26±0.01	51079.39	−0.33±0.01
51080.30	−0.30±0.01	51080.25	−0.28±0.01	51080.23	−0.43±0.01
51081.21	−0.15±0.02	51081.04	−0.06±0.01	51081.05	−0.09±0.01
		51082.47	0.12 ± 0.02	51082.50	−0.21±0.02
		51084.09	−0.13±0.02		
		51085.07	−0.16±0.03		
		51086.36	−0.11±0.03		

continuing decline to 14 mJy on MJD 51092, after which the monitoring ceased.

The ATCA started observing XTE J1550−564 on MJD 51073 while the flux density was still low, ∼8–16 mJy at all frequencies (Fig. 2). After the rise to 168 mJy detected with the MOST, the ATCA resumed observing the source and monitored it over the next 10 d. The ATCA flux densities range from 330.8 mJy at 1.4 GHz to 234.4 mJy at 8.6 GHz at the peak of the light curves, after which they then followed the same decline as the MOST, reaching a level of around 20 mJy at 4.8 GHz on MJD 51086.5 when monitoring ceased.

The bottom panel of Fig. 2 shows the evolution of two-point spectral indices α ($S_\nu \propto \nu^\alpha$) derived from the 1.4–4.8 GHz ($\alpha_{1.4-4.8}$) and the 4.8–8.6 GHz ($\alpha_{4.8-8.6}$) data. $\alpha_{1.4-4.8}$ varies between −0.28 and −0.12 and $\alpha_{4.8-8.6}$ between −0.43 and −0.09 (Table 2). The inset in the bottom panel shows the evolution of $\alpha_{1.4-4.8}$ and $\alpha_{4.8-8.6}$ in detail – for clarity in the main plot, the first five points were averaged for $\alpha_{1.4-4.8}$ and the first six points for $\alpha_{4.8-8.6}$.

2.2 Distance estimate using the H I spectrum

2.2.1 Observing details and data reduction

On 1998 September 22, we measured H I absorption towards XTE J1550−564. We employed three antennae of the ATCA, and set the correlator to produce 1024 channels over a bandwidth of 4 MHz centred on 1420 MHz. Two linear polarization products were recorded.

To provide an extragalactic reference, on 2000 April 5 and 10 we observed the source SUMSS J154816−564057 (see Fig. 1) using all six ATCA antennae and the same correlator setting. SUMSS J154816−564057 is 25 arcmin south-west of XTE J1550−564 at RA = $15^{\rm h}48^{\rm m}16\overset{\rm s}{.}5$, Dec. = $-56^\circ40'57''$ (J2000), and its flux density is 0.78 ± 0.04 Jy at 843 MHz. In both cases, the phase centre of the interferometer was positioned 1 arcmin to the south of the target source.

The data were flagged and calibrated with MIRIAD, following standard procedures. During reduction, the data were Hanning-smoothed and every other channel was discarded. The 512 channels in the resulting spectrum are separated by 1.65 km s^{-1}.

The spectra were obtained by shifting the phase centre of the array to the source position, and vector averaging the Stokes *I* visibilities (MIRIAD task UVSPEC). After several experiments with different choices of uv-data, baselines shorter than 2 kλ were excluded, in order to avoid artefacts caused by the nearby supernova remnant G326.3−1.8. Both scans of SUMSS J154816−564057 were averaged together, after intercomparison showed negligible differences between them. The continuum flux density of XTE J1550−564 was 0.280 ± 0.005 Jy and that of SUMSS J154816−564057 was 0.465 ± 0.002 Jy; the net on-source integration times (after flagging and uv-selection) were 60 and 132 min, respectively.

2.2.2 Interpretation

Fig. 3 shows the two H I absorption spectra superimposed: XTE J1550−564 in black and SUMSS J154816−564057 in grey. These spectra have been further Hanning-smoothed over three channels, with all channels retained. Several features have been identified, and listed in Table 3. The estimates of the Galactocentric radius and heliocentric distance to the clouds producing the absorptions are based on the Galactic rotation curve given by Fich, Blitz & Stark (1989).

Comparison of these spectra is complicated by significant differences in signal to noise. In the normalized units of Fig. 3, we estimate the rms noise to be 0.04 in the XTE J1550−564 spectrum and 0.013 in the SUMSS J154816−564057 spectrum. In the spectrum towards SUMSS J154816−56405, we are confident that all the features identified by letters A to H in Fig. 3 and Table 3 are absorptions produced by H I clouds along the line of sight, and not instrumental artefacts. In the spectrum towards XTE J1550−564, we have no hesitation in identifying the features near C, E and F as real absorptions, while the feature near B is marginally significant. However, we do not consider feature I or the feature near G to be strong enough to be considered real absorptions, given the noise level in the spectrum. Features D and H in SUMSS J154816–564057 are deep enough that, should the sightline towards XTE J1550−564 intersect gas from the same cloud under the same excitation conditions, we should have detected these absorptions above the noise.

The three clear H I absorptions found in the spectrum of XTE J1550−564 match well with corresponding features seen

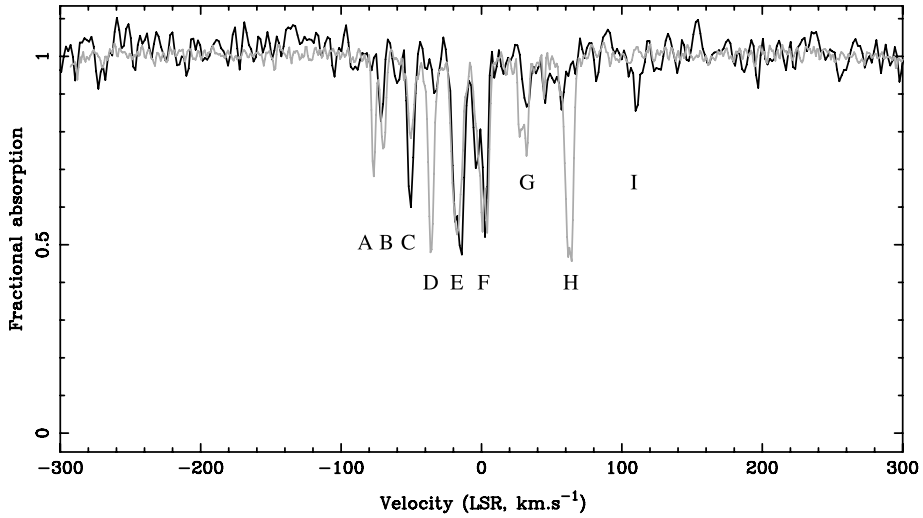

Figure 3. The H I spectrum of XTE J1550−564 represented in black and a spectrum taken towards SUMSS J154816−564057 in grey. Absorption of the continuum emission from XTE J1550−564 is seen clearly in the features labelled C, E and F.

Table 3. Features in the H I spectra of XTE J1550−564 and SUMSS J154816−564057.

$V_{\rm lsr}$ (km s^{-1})	$R_{\rm gal}$ (kpc)	Distance (kpc)	
SUMSS J154816−564057			
64.3	17.37	23.65	H
31.8	11.28	17.27	G
27.4	10.77	16.7	G
0.7	8.47	0.04	F
−16.2	7.46	1.3	E
−35.4	6.57	2.52	D
−50.1	6.02	3.37	C
−69.2	5.43	4.45	B
−76.3	5.24	4.88	A
XTE J1550−564			Id
110.4	69.9	76.8	I?
0.7:	8.46	0.04	F
−12.7	7.65	1.06	E
−49.2	6.05	3.32	C

in SUMSS J154816−564057. The velocity of feature F in XTE J1550−564 is uncertain but the overall profile match with SUMSS J154816−564057 is good, so we have adopted the same $V_{\rm lsr}$.

The observed absorptions allow us to constrain the distance to XTE J1550−564. The strongest constraint comes from feature C, which implies a distance greater than 3.3 kpc. However, the velocity of this feature is associated with two possible distances (as are all the features A–F). We believe that the far distance (10.6 kpc) for feature C is effectively ruled out by the absence of feature A (4.88 kpc). If XTE J1550−564 lies beyond 3.3 kpc, our non-detection of feature D (2.52 kpc) requires either that this sightline misses the cloud seen against SUMSS J154816−564057 or that there is a dearth of H I along this part of the sightline. Emission spectra at the position of XTE J1550−564 (McClure-Griffiths et al. 2005) show emission peaks at velocities matching the strong absorptions C, E and F, but weaker emission near −30 km s^{-1} suggesting there could indeed be a dearth of H I at the velocity corresponding to D. In setting an upper limit for the distance to XTE J1550−564, we prefer to use the absence of a counterpart to feature A (4.88 kpc) rather than argue over the reality of the feature near B (4.45 kpc).

In summary, we interpret the H I spectra as showing the distance to XTE J1550−564 is probably in the range 3.3–4.9 kpc. This puts the source slightly farther away than the estimate of 2.5 kpc based on the equivalent width of the Na D absorption line in the optical spectrum (Sanchez-Fernandez et al. 1999).

2.2.3 Possible association with G326.3−1.8

The overlap in distance between XTE J1550−564 (4.1 ± 0.8 kpc) and G326.3−1.8 (4.1 ± 0.7 kpc; Rosado et al. 1996) and their proximity in the plane of the sky raises the interesting question of a possible connection. Given the estimated age of the supernova remnant of $1.04 \pm 0.09 \times 10^4$ yr (Kassim, Hertz & Weiler 1993), we considered the possibility that XTE J1550−564 was ejected during the supernova explosion. The implied transverse velocity, however, is ∼3000 km s^{-1} which is implausibly high. We therefore conclude that XTE J1550−564 and G326.3−1.8 are not associated. Further evidence comes from *Chandra* and *XMM–Newton* observations that may have identified the pulsar and associated X-ray synchrotron nebula close to the radio plerion (Plucinsky et al. 2004).

2.3 LBA images

The LBA observations were carried out on 1998 September 24 (Epoch 1) and 1998 September 25/26 (Epoch 2) and are summarized in Table 4. Preliminary results and their interpretation were reported in Hannikainen et al. (2001). Note, however, that the mid-point MJDs quoted in that paper are erroneous, and we report the correct dates and times here. Fig. 4 shows the two LBA images at 2.29 GHz and Table 5 summarizes the flux densities of the components. The zero coordinate in the images is arbitrary, as phase-referenced observations were not performed on either day.

An additional component is seen in the image from Epoch 2 compared to Epoch 1, but as the image centre is arbitrary, it is not clear how the components are related. We note, however, that the ATCA two-point spectral indices start to flatten together right after the first LBA observation (Fig. 2). Shortly thereafter, the 4.8–8.6 GHz spectral index steepens again slightly, while the 1.4–4.8 GHz spectral index continues to flatten. The latter starts to steepen only some time during or after the second LBA observation.

Table 4. LBA observing log.

Date	T_{start} (UT)	T_{end} (UT)	Antenna	Frequency (GHz)
Epoch 1				
1998 September 24	02:50	06:00	DSS45 (34 m)	2.29 & 8.4
Mid-point:	51080.18		Hobart (26 m)	2.29 & 8.4
(MJD)			Mopra (22 m)	2.29
Epoch 2				
1998 September 25	22:30	09:00	DSS43 (70 m)	2.29 & 8.4
Mid-point:	51082.15		Hobart (26 m)	2.29 & 8.4
(MJD)			Mopra (22 m)	2.29
			ATCA (6 × 22 m)	2.29

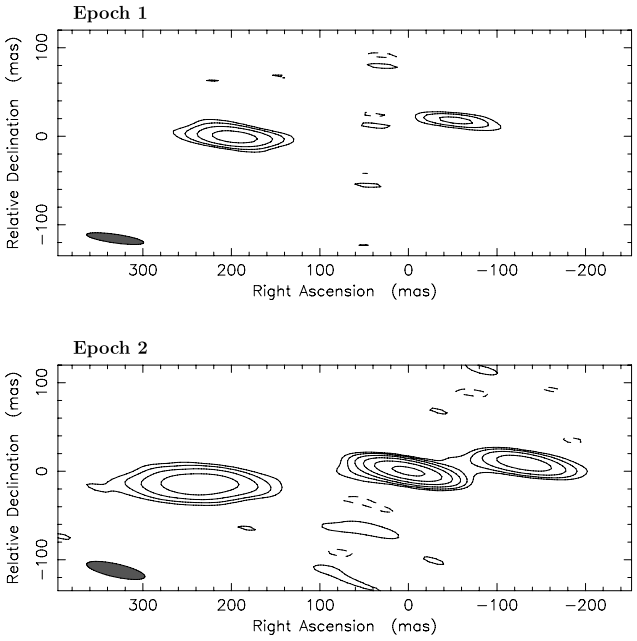

Figure 4. LBA images at 2.29 GHz from 1998 September 24 (Epoch 1, top) and 1998 September 25/26 (Epoch 2, bottom). The beam is shown in the lower left-hand corner. The zero coordinate is arbitrary. Reproduced from Hannikainen et al. (2001), with kind permission from Springer Science+Business Media: Astrophysics and Space Science Supplement, XTE J1550–564: a superluminal ejection during the September 1998 outburst, 276, 2001, 45, Hannikainen, Campbell-Wilson, Hunstead, McIntyre, Lovell, Reynolds, Tzioumis, Wu, Figure 1, © 2001 Kluwer Academic Publishers.

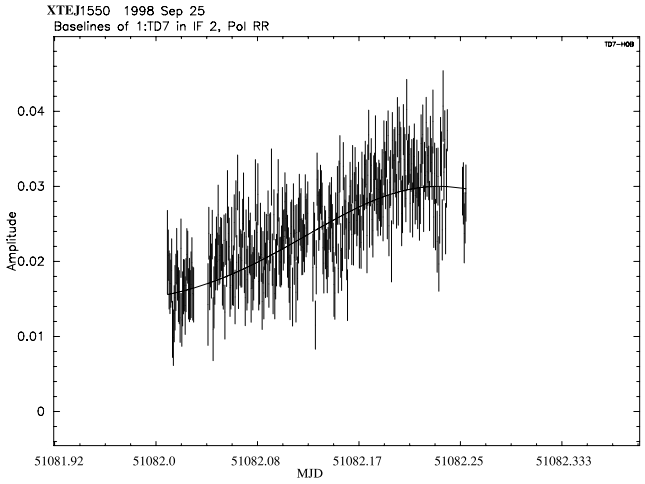

Figure 5. The observed visibility amplitudes on the DSS43-Hobart baseline at 8.4 GHz on 1998 September 25 (MJD 51082) and a fit of a simple source model consisting of a single elliptical Gaussian component (curve).

We infer, therefore, that a new outburst has occurred in XTE J1550−564 between Epoch 1 and Epoch 2 and associate the central component in the bottom panel of Fig. 4 with the flaring core and the two outer components with the ejecta seen in the top panel. Single baseline 8.4 GHz data from Epoch 2 (Fig. 5) show a new unresolved component not present in the data from Epoch 1, which supports this interpretation.

The increase in 8.4 GHz visibility amplitude on the DSS43-Hobart baseline peaked at MJD 51082.21 (Fig. 5). Such a change may be due to structure in the source and/or an intrinsic change in the source over the period of the observation. The peak in the visibility amplitude on this baseline corresponds to a position angle in the (u, v) plane of $6.5 \pm 3^\circ$ which, for a simple elongated source, corresponds to a position angle of the major axis in the image plane of $-83.5 \pm 3^\circ$, consistent with the position angles of the outer components at 2.29 GHz. Such a coincidence provides strong evidence that the variation in visibility can be explained by a resolved component at 8.4 GHz. Simple model fits to the data place an upper limit on the angular size of this component of ∼5 mas. This unambiguously identifies the central source as the core.

Table 5 shows the relative positions of the components in Fig. 4 at both epochs. For Epoch 1, the position of the weaker component (west) was measured with respect to the stronger component (east), while for Epoch 2 the positions of the outer components were measured with respect to the central component. The errors were estimated using DIFWRAP (Lovell 2000). The table also shows the position angles defined by the outer components. We note that Corbel et al. (2002) have found the same position angles from their observations in 2000 and 2002.

Table 5. Component positions and flux densities at 2.29 GHz. The uncertainties in the flux densities are of the order 10–20 per cent.

Date	Relative position (mas)		Position angle	Flux density (mJy)			Total
	East	West	(degrees)	East	Central	West	(mJy)
Epoch 1	200[a]	55[a]	$-86.1^{+1.5}_{-0.9}$	71	—	20	91
Epoch 2	254^{+15}_{-12}	130 ± 12	-86.1 ± 0.8	19	25	8	52

[a]Positions measured relative to an arbitrary origin. Component separation is 255^{+15}_{-19} mas.

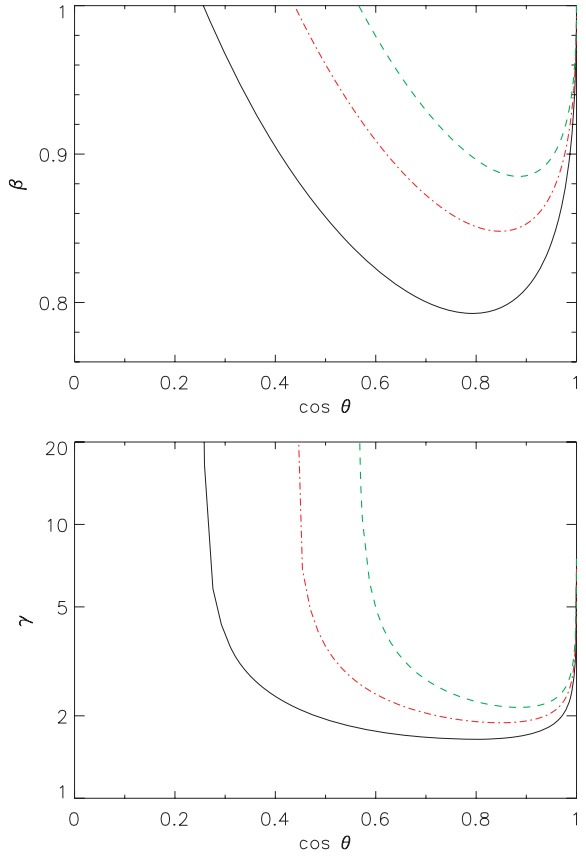

Figure 6. The top panel shows the inferred separation velocity of the ejecta, β, for various viewing angles, θ, and the bottom panel shows the corresponding γ for $v = 1.3c$ (solid black), $1.6c$ (dot–dash red) and $1.9c$ (dash green).

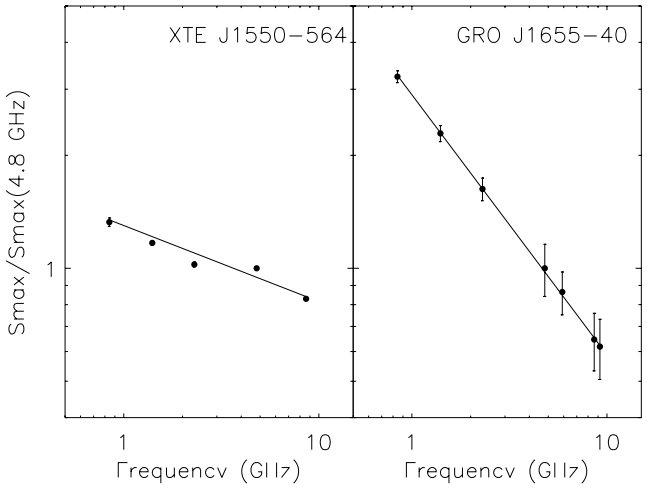

Figure 7. Flaring amplitudes for XTE J1550−564 (left) and GRO J1655−40 (right; from Stevens et al. 2003). The slopes of the power laws are −0.2 and −0.7, respectively.

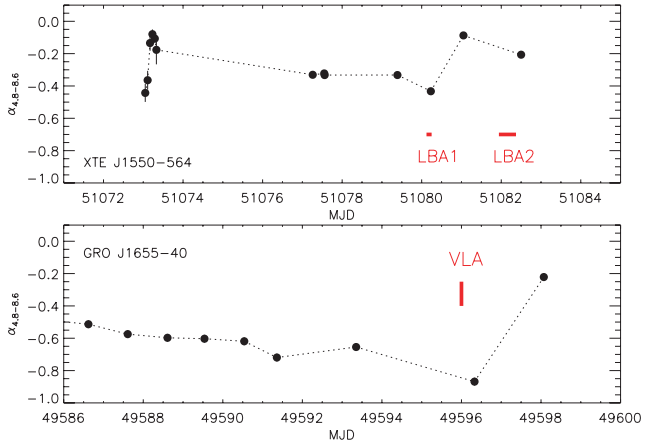

Figure 8. Two-point (84.8–8.6 GHz) spectral indices as a function of time for XTE J1550−564 (top) and GRO J1655−40 (bottom). Marked in the top panel are the epochs of the LBA observations shown in Fig. 4 and, in the bottom panel, the onset of a major ejection event in GRO J1655−40 seen with the Very Large Array (VLA) (Hjellming & Rupen 1995).

On the basis of the above interpretation, the ejecta have moved apart by approximately 130 mas in ∼2 d. At the closer distance of 3.3 kpc, this implies an apparent separation velocity of $1.3c$ for the ejecta, while for the farther distance of 4.9 kpc the separation velocity is $1.9c$.

Fig. 6 shows the inferred separation velocity of the ejecta, β, and the corresponding γ for various viewing angles, θ, for three apparent ejecta velocities: $1.3c$, $1.6c$, and $1.9c$. Thus, β is at least greater than 0.8 and γ is at least greater than 1.6.

3 XTE J1550−564 AND GRO J1655−40

At least five Galactic sources are known to have exhibited apparent superluminal motion: GRS 1915+105 (Mirabel & Rodríguez 1994), GRO J1655−40 (Tingay et al. 1995; Hjellming & Rupen 1995), XTE J1748−288 (Hjellming et al. 1998), SAX J1819.3−2525 (V4641 Sgr; Hjellming et al. 2000) and XTE J1550−564. All five sources displayed very different multiwavelength behaviour at the time of the ejection outbursts, and in the evolution of the ejecta themselves. However, there are several similarities in the multi-frequency data for XTE J1550−564 and GRO J1655−40 that we discuss below.

The most obvious similarity between the radio properties of XTE J1550−564 and GRO J1655−40 is the high expansion velocity of the ejecta, $\geq 0.8c$ for XTE J1550−564 and $\sim 0.9c$ for GRO J1655−40 at respective distance estimates of $3.3 < d < 4.9$ kpc and ∼3.2 kpc. In addition, the behaviour during the radio outburst is very similar, as can be seen when comparing the flux density light curves. In GRO J1655−40, the light curves at all frequencies rise and fall simultaneously, with the lowest frequencies peaking with the highest flux densities. The flux density light curves of XTE J1550−564 appear to peak simultaneously (Fig. 2, top panel). Due to lack of simultaneous coverage in the observed frequencies, we cannot say with certainty that they peaked at the same time. However, it is apparent that, as with GRO J1655−40, the flare amplitudes, normalized to 4.8 GHz, increase towards lower frequency as shown in Fig. 7, albeit with a shallower slope, the power-law index being −0.2 as opposed to −0.7 for GRO J1655−40.

Fig. 8 shows the temporal evolution of two-point spectral indices in both XTE J1550−564 and GRO J1655−40 during the times of their respective ejection events. Although the coverage for GRO J1655−40 was more complete, the figure shows that in both sources, at the time of a major recorded ejection event in GRO J1655−40 and during the LBA-recorded ejection event in XTE J1550−564, the 4.8–8.6 GHz two-point spectral index showed a significant flattening.

4 SUMMARY

We confirm the presence of apparent superluminal motion from XTE J1550−564 during its 1998 September outburst. Comparison between the H I absorption spectra towards XTE J1550−564 and the nearby extragalactic source SUMSS J154816−564057 has allowed us to constrain the distance to XTE J1550−564 to lie between 3.3 and 4.9 kpc. Based on two-epoch observations with the Australian LBA, these distances yielded apparent separation velocities of the ejecta of 1.3c at the closer distance and 1.9c at the farther distance. After correcting for relativistic effects this leads to an intrinsic ejection velocity $\geq$0.8c. The maximum flux density during the 1998 September outburst was 375 mJy at 843 MHz and ranged from ∼330 mJy to ∼234 mJy at 1.4 and 8.6 GHz, respectively. As with the superluminal source GRO J1655−40, the flux densities appear to peak simultaneously at all frequencies, but with a much flatter (but optically thin) spectral index of −0.2 compared with −0.7 for GRO J1655−40. In addition, the spectral evolution during the outburst is reminiscent of that observed in GRO J1655−40 during its 1994 outburst.

ACKNOWLEDGMENTS

The authors thank Robert Braun and Jim Caswell for helpful discussions on the distance to XTE J1550−564. MOST is operated by the University of Sydney and supported by grants from the Australian Research Council. The ATCA and the Mopra Telescope are part of the Australia Telescope which is funded by the Commonwealth of Australia for operation as a National Facility managed by CSIRO. We thank the staff of both the University of Tasmania and the Canberra Deep Space Communications Complex, Tidbinbilla. DCH gratefully acknowledges the Academy of Finland for a Fellowship and project number 212656.

REFERENCES

Beloborodov A. M., Illarionov A. E., 2001, MNRAS, 323, 167
Campbell-Wilson D., McIntyre V., Hunstead R. W., Green A., 1998, IAU Circulars, 7010
Corbel S. et al., 2001, ApJ, 554, 43
Corbel S., Fender R. P., Tzioumis A. K., Tomsick J. A., Orosz J. A., Miller J. M., Wijnands R., Kaaret P., 2002, Sci, 298, 196
Corbel S., Tomsick J. A., Kaaret P., 2006, ApJ, 636, 971
Cui W., Zhang S. N., Chen W., Morgan E. H., 1999, ApJ, 512, L43
Fich M., Blitz L., Stark A. A., 1989, ApJ, 342, 272
Hannikainen D., Campbell-Wilson D., Hunstead R., McIntyre V., Lovell J., Reynolds J., Tzioumis T., Wu K., 2001, Ap&S Supp., 276, 45
Hjellming R. M., Rupen M. P., 1995, Nat, 375, 464
Hjellming R. M., Rupen M. P., Mioduszewski A. J., Smith D. A., Harmon B. A., Waltman E. B., Ghigo F. D., Pooley G. G., 1998, American Astron. Soc. Meeting 193, 103.08
Hjellming R. M. et al., 2000, ApJ, 544, 977
Homan J., Wijnands R., van der Klis M., Belloni T., van Paradijs J., Klein-Wolt M., Fender R., Méndez M., 2001, ApJS, 132, 377
Jain R. K., Bailyn C. D., Orosz J. A., McClintock J. E., Sobczak G. J., Remillard R. A., 2001, ApJ, 546, 1086
Kaaret P., Corbel S., Tomsick J. A., Fender R., Miller J. M., Orosz J. A., Tzioumis A. K., Wijnands R., 2003, ApJ, 582, 945
Kassim N. E., Hertz P., Weiler K. W., 1993, ApJ, 419, 733
Kubota A., Done C., 2004, MNRAS, 353, 980
Lovell J., 2000, in Hirabayashi H., Edwards P. G., Murphy D. W., eds, Astrophysical Phenomena Revealed by Space VLBI. ISAS, Sagamihara, p. 301
McClure-Griffiths N. M., Dickey J. M., Gaensler B. M., Green A. J., Haverkorn M., Strasser S., 2005, ApJS, 158, 178
Mills B. Y., 1981, Publ. Astron. Soc. Aust., 4, 156
Mirabel I. F., Rodríguez L. F., 1994, Nat, 371, 46
Orosz J. A., Bailyn C. D., Jain R. K., 1998, IAU Circulars, 7009
Orosz J. A. et al., 2002, ApJ, 568, 845
Plucinsky P. P., Dickel J. R., Slane P. O., Gaetz T. J., Sasaki M., Edgar R. J., Smith R. K., 2004, American Astron. Soc. Meeting 205, 106.13
Remillard R., Morgan E., McClintock J., Sobczak G., 1998, IAU Circulars, 7019
Robertson J. G., 1991, Aust. J. Phys., 44, 729
Rosado M., Ambrocio-Cruz P., Le Coarer E., Marcelin M., 1996, A&A, 315, 243
Sanchez-Fernandez C. et al., 1999, A&A, 348, L9
Smith D. A., 1998, IAU Circulars, 7008
Smith D. A., Heindl W. A., Swank J. H., 2002, ApJ, 569, 362
Sobczak G., McClintock J. E., Remillard R. E., Levine A. M., Morgan E. H., Bailyn C. D., Orosz J. A., 1999, ApJ, 517, L121
Stevens J. A., Hannikainen D. C., Wu K., Hunstead R. W., McKay D., 2003, MNRAS, 342, 623
Tingay S. J. et al., 1995, Nat, 374, 141
Titarchuk L., Shrader C. R., 2002, ApJ, 567, 1057
Tomsick J. A., Corbel S., Fender R., Miller J. M., Orosz J. A., Tzioumis A. K., Wijnands R., Kaaret P., 2003, ApJ, 582, 933
Wang X. Y., Dai Z. G., Lu T., 2003, ApJ, 592, 347
Whiteoak J. B. Z., Green A., 1996, A&AS, 118, 329
Wijnands R., Homan J., van der Klis M., 1999, ApJ, 526, L33
Wilson C. A., Harmon B. A., Paciesas W. S., McCollough M. L., 1998, IAU Circulars, 7010
Wu K. et al., 2002, ApJ, 565, 1161
Wu Y. X., Liu C.-Z., Li T.-P., 2007, ApJ, 660, 1386
Xue Y., Wu X.-B., Cui W., 2008, MNRAS, 384, 440

This paper has been typeset from a TEX/LATEX file prepared by the author.